

Multiscale Interaction Between a Cluster of Buildings and the ABL Developing Over a Real Terrain.

Marcel Vonlanthen^{a,b,*}, Jonas Allegrini^{a,b}, Jan Carmeliet^{a,b}

^aChair of Building Physics, Swiss Federal Institute of Technology of Zurich, ETHZ, Zurich, Switzerland

^bLaboratory for Multiscale Studies in Building Physics, Swiss Federal Laboratories for Material Testing and Research, Empa, Dübendorf, Switzerland

Abstract

A nested Large Eddy Simulation (LES) is used to compute the multiscale interaction between the Atmospheric Boundary Layer (ABL) and an existing cluster of buildings over the real topography. A Neutral ABL (NBL) and a Convective ABL (CBL) are simulated. As the ABLs develop over an no-flat terrain with heterogeneous roughness elements, standard ABL-LES with cyclic boundary condition can not be used. Instead, a synthetic inflow generator is used to generate realistic turbulent NBL and CBL over the real terrain. The outer domain of the nested-LES is dedicated to solve the ABL flow, with the building parametrized with a rough wall model, whereas the inner domain computes the flow through the cluster of buildings. Both LES are connected with a one-way downscale nesting procedure. The effects of the NBL and the CBL are clearly visible at building scale. The horizontal turbulent flux and the vertical turbulent flux are enhanced in the CBL compared to the NBL. The temperature difference between the air within the cluster of buildings and the rural surrounding is similar for both ABL condition, even if the turbulent mixing is higher in the CBL case. We further show that the critical part of the nested simulation is the ability of the ABL-LES to properly compute the roughness layer near the ground. Current rough wall models used to parametrize urban area are not able to reproduce such layer, which can negatively impact the flow inside the building-resolved LES.

Keywords: Large Eddy Simulation, Multiscale, Microclimate, Nesting, Wind Engineering, Urban Flows, Wall Model

1. Introduction

The interaction between the turbulent eddies generated by a cluster of buildings and the turbulent Atmospheric Boundary Layer (ABL) developing over a realistic terrain covers several orders of magnitude. The turbulent structure in a ABL have a size extending from $1 \cdot 10^2$ m to $1 \cdot 10^3$ m, whereas the eddies developing in the wake of a building have a typical lengthscale of 1 m to 10 m (Wyngaard, 2010). Those two range of scales, namely the ABL scales and the building scales, have been studied with Large Eddy Simulation (LES).

The flow in a ABL is turbulent, with a strong anisotropy in the vertical direction. This anisotropy is mainly due to buoyancy effect. The air warmed up by the hot ground generates an unstable situation, and starts to rise. This vertical motion is organized in so-called thermals and participate to the strong mixing capabilities, which characterizes ABLs. Due to its turbulent and anisotropic nature, ABLs are generally simulated with LES. Moeng (1984), Sullivan et al. (1994) and Sullivan et al. (1996) performed in their work the first LES's of Neutral ABL (NBL) and Convective ABL (CBL) over flat and homogeneous terrain. In general, such LES of ABL cover several square kilometer of terrain, from $3 \text{ km} \times 3 \text{ km}$ to $10 \text{ km} \times 10 \text{ km}$, with a vertical extend from 1 km to 2 km. The typical mesh for such domain is composed of cells of 10 m to 30 m in size. As the terrain is flat and homogeneous, cyclic side boundary condition can

*corresponding author

Email addresses: vonlanthen@arch.ethz.ch (Marcel Vonlanthen), jonas.allegrini@empa.ch (Jonas Allegrini), carmeliet@arch.ethz.ch (Jan Carmeliet)

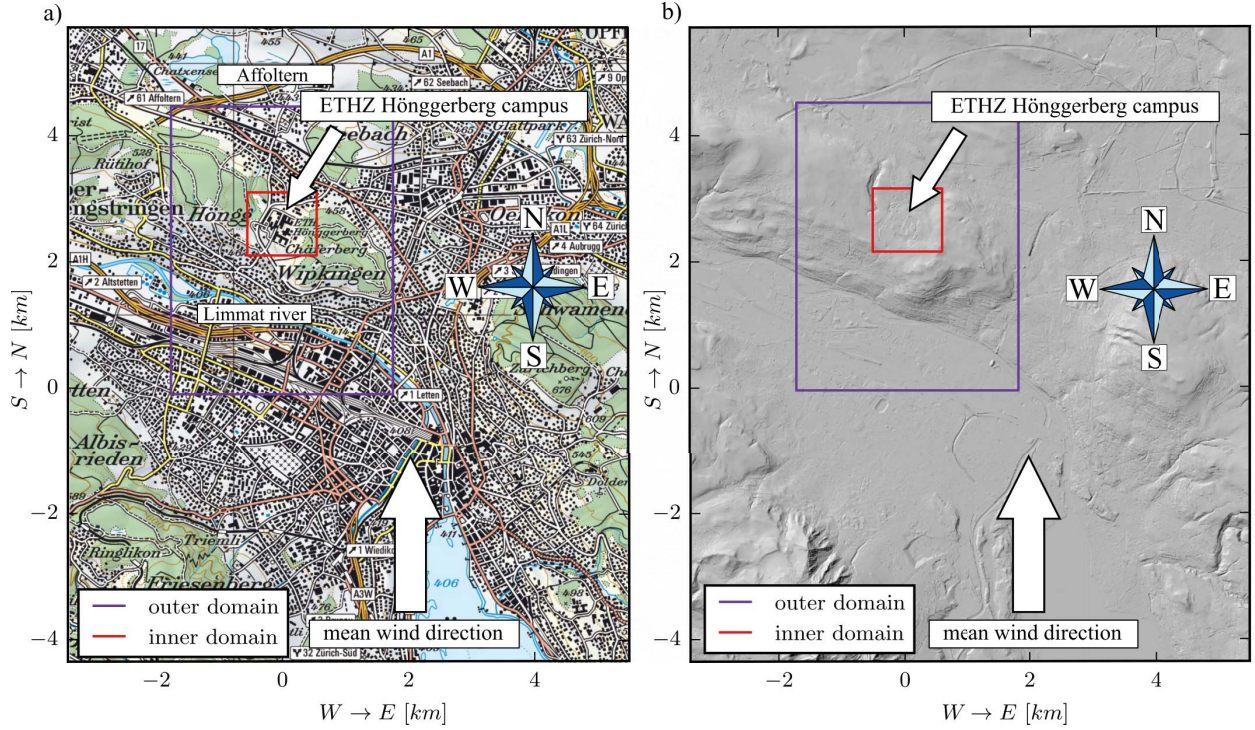


Figure 1: Topographic map (a) and elevation map (b) of the city of Zurich. The location of the outer and the inner domain are highlighted in purple and red respectively. Topographic map reproduced by permission of swisstopo (BA16022).

be used and the Coriolis force is included in the momentum equation. The flow is driven either by a constant pressure gradient or by a geostrophic wind applied at the top boundary of the domain.

In this study, we use the state-of-the-art ABL simulation and building-resolved simulation to compute the flow within an existing cluster of buildings under the influence of a NBL and a CBL. Due to the wide range of turbulent scales, we use a nesting procedure. The large ABL scales are resolved in a dedicated Large-scale LES (L-LES) whereas the turbulent flow around the buildings is resolved by a Small-scale LES (S-LES). The L-LES is also known as the *outer domain* and the S-LES the *inner domain*. As the buildings are located in an environment with a complex topography, we can not use a cyclic condition in the ABL simulation to let the turbulence develop “naturally” over the terrain. To generate a proper turbulent ABL over the complex topography, we use the synthetic inflow generator proposed by [Xie and Castro \(2008\)](#). Such inflow generator needs the statistics (mean, variance and lengthscale) of the NBL and CBL we want to impose at the inlet. The statistics are extracted from two state-of-the-art LES of a NBL and a CBL over a flat and homogeneous terrain.

This paper is organized as follows. the building geometry and the terrain topography are presented in Section 2. The setup of the outer and the inner domain is presented in Section 3 and 4. The Section 5 describes in detail the nesting procedure and the solver setup. The simulations used to generate the flow statistics for the synthetic inflow generator are presented in Section 6. The results of the nested simulations are shown in Section 7 and a discussion on the results is proposed in Section 8. Finally, the Section 9 gives the main conclusion.

2. Topology and geometry

The Hönggerberg campus is one of the two campus of the Swiss Federal Institute of Technology of Zurich - ETH Zurich. The campus sits on a shallow pass of the Hönggerberg hill (Fig.1). It is surrounded on its NW-SE axis by two dense and mature forests of broad-leaf trees. The hill is bordered on the SW by the alluvial plain of the river Limmat. The plain is densely urbanized with low raise buildings rarely taller than 50 m. On the NE of the hill stretches the relatively flat, mixed rural-urbanized area of Affoltern. The city-center of Zurich is located ≈ 4 km NW of the

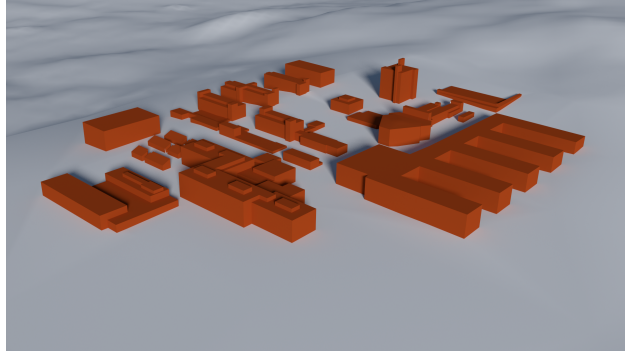


Figure 2: Geometry used for the ETH Hönggerberg campus. View from the south-west with late afternoon sun.

campus. Zurich is a typical European city, with densely packed low-raise buildings. The northern tip of the lake of Zurich is located roughly 5 km south of the campus.

The campus itself is a cluster of about 20 heterogeneous buildings as it can be seen in Figure 2. It is relatively isolated from other constructions and surrounded by mostly green surfaces (forest or crop). The footprint of the campus can be approximated by a square of 600 m by 600 m. Most of the buildings have an horizontal extend of $\approx 60 \text{ m} \times 60 \text{ m}$, with the notable exception of the southern most building, with a comb-like shape, which has a footprint of $\approx 100 \text{ m} \times 26 \text{ m}$. The average height of the buildings is $\approx 25 \text{ m}$.

The flow through the campus is strongly influenced by the hill and the surrounding inhomogeneous roughness elements (forest, crops, city blocs). Therefore, standard ABL profiles (Richards and Norris, 2011) cannot be used to feed a synthetic inflow generator, because they are derived on the hypothesis of flat and homogeneous terrain. Therefore a large computational domain would be needed to take into account the effects of the roughness and topology on the ABL. But if the large domain includes well-resolved buildings, the timestep to account the very small cell near the buildings should be extremely small. Such single domain LES would become computationally expensive as a lot of computational time would be *wasted* in simulating the large turbulent structures of the ABL with an unnecessary small timestep. Therefore a nesting procedure is used in this study. The outer domain is dedicated to compute the ABL only, the roughness elements being parametrized by a wall-model. The inner domain computes only the flow through the campus, which is discretized by a well-resolved grid. The arrangement of both domains is shown in Figure 1.

3. Model setup and boundary conditions

3.1. Outer domain

As visible in Figure 1 and 3, the outer domain covers 4560 m in the NS direction and 3520 m in the EW direction. The Hönggerberg campus is located roughly in the middle of the outer domain and the campus buildings are parametrized by a wall function. The lowest topographic point included in the domain is at 391 m Above Mean Sea Level (AMSL) and the highest point is 565 m. The average elevation of the campus is 524 m AMSL. In the vertical direction, the outer computational domain extends up to 3810 m AMSL, which is $\approx 3350 \text{ m}$ above the average ground level of the region. The height of the domain is chosen to avoid too strong blockage due to the hill. With such land cover, the domain covers a large part of the two forests surrounding the campus, as well as a part of the city located SW from it. The general dimensions of the domain are selected according to the best practice for LES of ABL (Moeng, 1984, Sullivan et al., 1996, Noh et al., 2003, Botnick and Fedorovich, 2008).

The outer computational domain is selected to simulate a neutral ABL with a height of 800 m AGL and a mean wind direction from the South. This particular wind direction is selected to take into account the capabilities of synthetic inflow generators. Indeed, an inflow generator needs the statistics (i.e. mean velocity, Reynolds stress and lengthscale) as input to reproduce the turbulent flow. To compute these statistics several methods are available, which are valid only for flat and homogeneous terrain for the most of them:

- Statistics and the lengthscales can be computed from standard profiles (Richards and Norris, 2011) or similarity laws (Holtslag and Nieuwstadt, 1986, Kaimal, 1973).

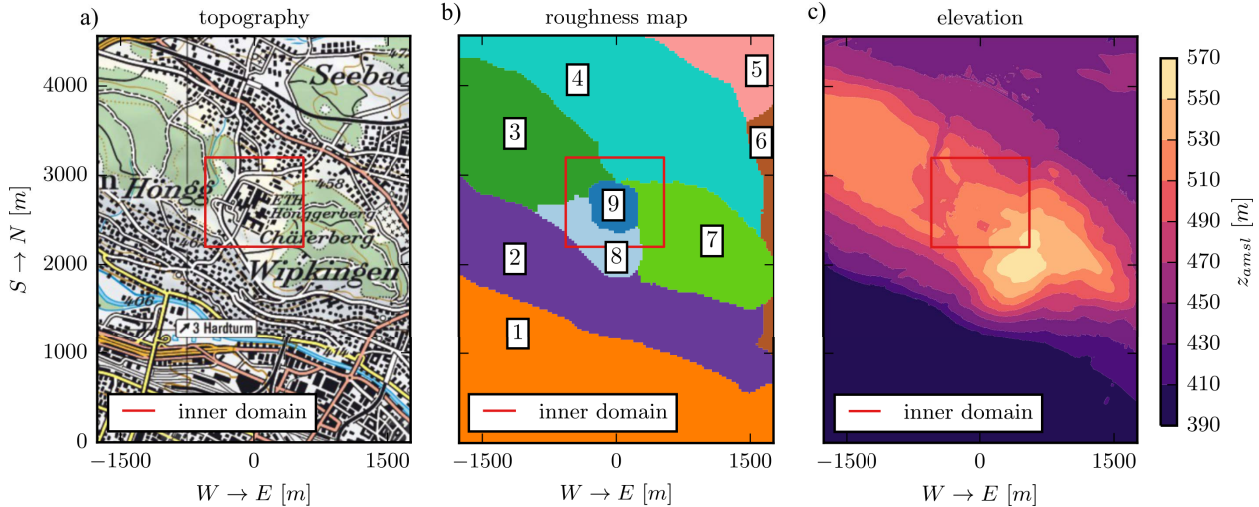


Figure 3: Ground cover of the computational domain. Topography from the Federal Office of Topography - SwissTopo.

- Statistics can be extracted from a mesoscale Numerical Weather Prediction (NWP) simulation. As all NWP model are based on the RANS equations at best (some use the Euler equations), the turbulent lengthscales need to be approximated with algebraic models.
- Statistics and the lengthscales can be computed from a state-of-the-art LES of an ABL ([Moeng, 1984](#), [Botnick and Fedorovich, 2008](#)).

In the first method, the profiles are constructed with the hypothesis of flat and homogeneous terrain. The second method can provides realistic profiles on non flat and heterogeneous terrain but the resolution is quite poor. Mesoscale NWP models used by European meteorological offices have a typical resolution of $2 \times 2 \text{ km}$ to $5 \times 5 \text{ km}$ in the horizontal direction, with only a few cells are located in the ABL itself. The last method uses a LES to generate the statistics on an homogeneous and flat terrain. As LES are turbulence resolved, the lengthscales can be directly computed from the data, without implying algebraic approximations. For this test case, a state-of-the-art LES of an ABL is used to generate the data for the synthetic inflow generator used at the south boundary of the outer domain. Therefore the location of the inlet boundary condition of the outer domain has to be located in a relatively flat area with a homogeneous ground cover. This explain the choice of the flat alluvial plain of the Limmat river. For other wind directions, like a west wind, data from a mesoscale NWP would be the most suitable approach as the statistics would suit the topology and the roughness inhomogeneities.

The terrain covered by the outer domain is inhomogeneous. To take into account the various roughnesses, it is split in 9 patches (see Fig.3b). Every patch is modeled by the LES wall-model proposed by [Schumann \(1975\)](#). Table 1 gives the roughness length attributed to each patch. The roughness lengths have been chosen according the tables given by [Davenport \(1960\)](#) and [Wieringa \(1992\)](#). As the topology at the side boundaries is not the same, the east and west boundaries are set as free-slip wall. The top boundary is defined as free-slip and a zero velocity gradient is applied at the north boundary (outlet).

As it usually done in weather simulations (ABL or mesoscale), the potential temperature Θ is used to describe the air temperature, as well as the surface temperature. Θ is equivalent to T on small vertical extends, such as buildings. In the following, the word *temperature* is used instead *potential temperature* for simplicity. The surface temperature of the campus patch is set to 340 K in both NBL and CBL. This quite high value is close to simulated surface temperature in a cluster of building during a hot sunny day ([Allegrini et al., 2015](#)). The surface temperature of the other patches is set to 300 K in the NBL and 306 K for the CBL. 306 K is a common value used in literature to simulate an convective ABL on large scales. The temperature profile applied at the south boundary (the inlet) is extracted from the ABL-LES used to generate the statistics for the synthetic inflow generator. Zero temperature gradient is applied to the east, west, north and top boundaries.

The table 2 summarizes the boundary conditions applied to the L-LES.

index	patch name	z_0	description
1	downtown	1.5	Large obstacles with open spaces half the size of the characteristic height
2	Höngg	1.0	Large obstacles with open spaces comparable the characteristic height
3	Höngg forest	1.0	Mature forest
4	Affoltern	1.0	Same as Höngg (2)
5	Chatzensee	0.5	Cultivated landscape with large obstacles separated by open space 5 to 10 time larger than the characteristic height
6	Zurich north	1.2	Same as Höngg (2), but slightly more packed
7	Chäferberg	1.0	Mature forest
8	campus front	0.25	low crops or pasture with scattered obstacles
9	campus	1.2	Same as Höngg (2), but slightly more packed

Table 1: Roughness length z_0 attributed to each patches. The patch index are shown in Figure 3.

boundary	velocity u_i [m/s]	kinematic pressure p_k [Pa]	temperature Θ [K]
south (inlet)	$u_i = u_i^{IG}$	$\partial p_k / \partial x_i = 0$	$\Theta = \Theta^{IG}$
north (outlet)	$\partial u_i / \partial x_i = 0$	$p_k = 1 \times 10^5$	$\partial \Theta / \partial x_i = 0$
east (symmetric)	$\partial u_i / \partial x_2 = 0, u_2 = 0$	$\partial p_k / \partial x_2 = 0$	$\partial \Theta / \partial x_2 = 0$
west (symmetric)	$\partial u_i / \partial x_2 = 0, u_2 = 0$	$\partial p_k / \partial x_2 = 0$	$\partial \Theta / \partial x_2 = 0$
top (symmetric)	$\partial u_i / \partial x_3 = 0, u_3 = 0$	$\partial p_k / \partial x_3 = 0$	$\partial \Theta / \partial x_3 = 0$
ground	$u_i = 0$	$\partial p_k / \partial x_i = 0$	$\Theta^{NBL} = 300, \Theta^{CBL} = 306$
building (modeled)	$u_i = 0$	$\partial p_k / \partial x_i = 0$	$\Theta = 340$

Table 2: Boundary condition applied to the L-LES. The subscribe $.IG$ describes quantities generated by the synthetic inflow generator. The inflow generator uses as input the velocity and temperature profiles of the LES of a ABL over a flat terrain described in Section 6.

3.2. Inner domain

The inner domain is dedicated to simulate the turbulent flow through the campus. The ground footprint of the buildings, the land usage and the topology of the terrain are shown in Figure 4. The red box in Figure 3 shows its location inside the outer one. The inner domain covers 1000m of terrain in the NS direction and 1100m in the EW direction. The campus itself is located in the middle of the domain. The top of the domain is located 1200m AMSL, which is approximatively 670m AGL.

The ground of the S-LES domain represents a subset of the ground boundary in the L-LES. It means that both grounds are identical (in term of topology of the terrain), except for the buildings, which are resolved in the S-LES. Therefore the roughness length can be set to zero in the "campus" patch of the S-LES, as the buildings are the roughness elements themselves. The other patches have the same roughness length than their equivalent in the L-LES (see Table 1). The temperature of the ground patches no.3, 4, 7 and 8 is set to 300 K in the NBL and to 306 K in the CBL. The buildings and the campus patch (no.9) are set to 340K, as in the L-LES.

The south, east, west and top boundaries are the nested boundaries. They are coupled to the outer domain via the velocity and the temperature. The north boundary is not modeled as a nested boundary. The reason for this choice will be detailed in Section 8. Therefore zero velocity and temperature gradient are applied at the north boundary.

The table 3 summarizes the velocity, kinematic pressure and temperature boundary conditions applied to the S-LES.

4. Grid

The grid of the outer domain is presented in Figure 5. The grid is made of a base layer L_0 and two refinement layer L_1 and L_2 . Each layer covers the entire horizontal extend of the domain. The cells of each layer are cubical and their size is constant in a given layer. The transition between two refinement layers is sharp: a cell of the level L_{i+1} is

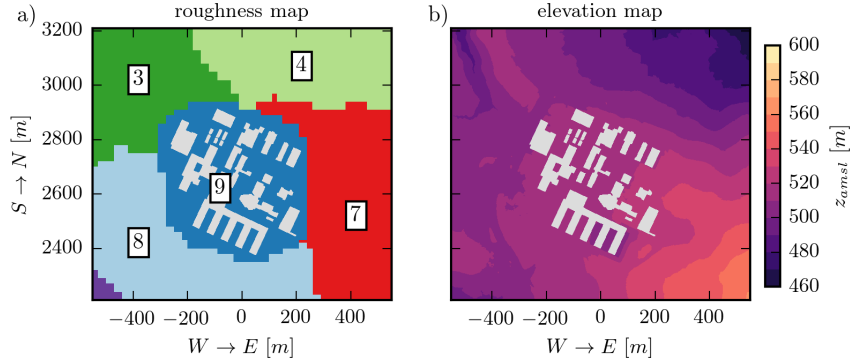


Figure 4: Inner computational domain with the building footprints (light gray), roughness map (a) and AMSL elevation (b).

boundary	velocity u_i [m/s]	kinematic pressure p_k [Pa]	temperature Θ [K]
S, E, W and top	$u_i = u_i^L$	$p_k = p_k^L$	$\Theta = \Theta^L$
north (outlet)	$\partial u_i / \partial x_i = 0$	$\partial p_k / \partial x_i = 0$	$\partial \Theta / \partial x_i = 0$
ground	$u_i = 0$	$\partial p_k / \partial x_i = 0$	$\Theta^{NBL} = 300$, $\Theta^{CBL} = 306$
building (resolved)	$u_i = 0$	$\partial p_k / \partial x_i = 0$	$\Theta = 340$

Table 3: Boundary condition applied to the S-LES. The subscript L describes the quantities interpolated from the L-LES.

twice smaller in all three directions than a cell from the level L_i . The grid of the inner domain is shown in Figure 6. It is composed of 4 level of refinements. The coarser levels L_1 and L_2 of the inner domain are the same as in the outer domain. The size of each level is given in Table 4.

In total, the grids of the outer and the inner domain are made of 4.23 and 2.03 million cells respectively. In the campus area, the grid ratio between the outer and the inner domain is equal to $L_2/L_5 = 8$.

5. Solver setup, nesting characteristics and boundary conditions

The outer and the inner domain are coupled with a one-way LES-to-LES nesting procedure. The filtered (or resolved) velocity \bar{u} , the filtered potential temperature $\bar{\Theta}$ and the filtered kinematic pressure \bar{p}_k are defined as:

$$\bar{u}_i = u_i - u''_i \quad (1a)$$

$$\bar{\Theta} = \Theta - \Theta'' \quad (1b)$$

$$\bar{p}_k = p_k - p''_k \quad (1c)$$

where u_i , Θ and p_k are the non-filtered velocity, potential temperature and kinematic pressure respectively. u''_i , Θ'' and p''_k are the sub-grid scale (sgs) velocity, potential temperature and kinematic pressure respectively. The index $i \in [1, 2, 3]$ represents the spatial directions, where x_1 is the south-north direction, x_2 the east-west direction and x_3 the vertical direction. In the outer domain, the standard filtered Navier-Stokes equations for incompressible flow are solved. The Boussinesq approximation for buoyancy is used to model the convective effects. The conservation of

refinement level	L_0	L_1	L_2	L_3	L_4	L_5
cell size in direction x_i [m]	40	20	10	5	2.5	1.25

Table 4: Cell for each refinement level composing the grids of the outer and the inner domain. The dimensions are given in meters.

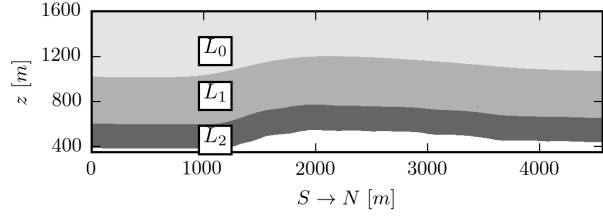


Figure 5: Grid of the outer domain. Only the lower part up to 1600m is shown. The level L_0 extends up to the top of the domain.

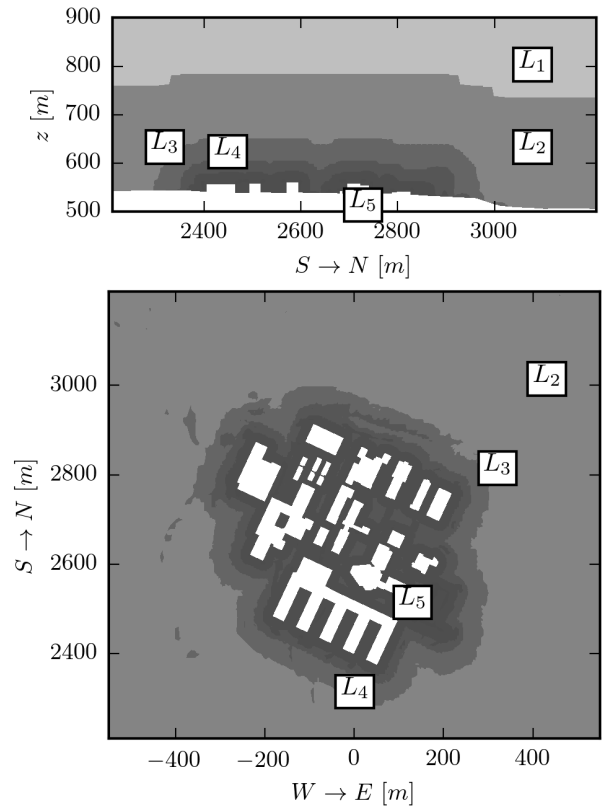


Figure 6: Grid of the inner domain. a) is a vertical cut at $EW = 0m$ and b) is a terrain following surface at $z = 10m$ AGL. Only the lower part up to 900m is shown. The level L_1 extends up to the top of the domain.

mass and momentum read as:

$$\frac{\partial \bar{u}_i^L}{\partial x_i} = 0 \quad (2)$$

$$\begin{aligned} \frac{\partial \bar{u}_i^L}{\partial t} + \bar{u}_j^L \frac{\partial \bar{u}_i^L}{\partial x_j} &= -\frac{1}{\rho_0} \frac{\partial \bar{p}_k^L}{\partial x_i} + \nu \frac{\partial^2 \bar{u}_i^L}{\partial x_j \partial x_j} - \frac{\partial \tau_{ij}^L}{\partial x_j} \\ &\quad + (1 - \beta (\bar{\Theta}^L - \bar{\Theta}_0^L)) g_i \end{aligned} \quad (3)$$

where ρ_0 is the reference density, β the thermal expansion coefficient, ν the dynamic viscosity and g_i the gravity. The superscript L described the quantities of the L-LES. For all equations, the Einstein notation is used. The pressure \bar{p} can be computed from the kinematic pressure \bar{p}_k with the following relation:

$$\bar{p}^L = \bar{p}_k^L + \rho_0 g_i h. \quad (4)$$

The Coriolis force, which is responsible of the rotation of the mean velocity vector in the upper part of the ABL, is not included in Eq.3. Indeed, as the terrain is not flat, cyclic boundary conditions cannot be used for the side boundaries, as it usually done in LES of ABL over flat terrain. Therefore the rotation of the flow with the altitude can not be handled without cyclic boundaries. Nevertheless, the Coriolis effect start to be important a few hundreds of meters above the ground level, therefore this assumption is not problematic for building-resolved studies. The sub-grid stress (sgs) tensor τ_{ij} is defined as

$$\tau_{ij} = \bar{u}_i \bar{u}_j - \bar{u}_i \bar{u}_j. \quad (5)$$

τ_{ij} is approximated by the eddy viscosity assumption

$$\tau_{ij} = \frac{1}{3} \delta_{ij} \tau_{kk} + \nu_{sgs} \bar{S}_{ij} \quad (6)$$

where ν_{sgs} is the sgs-viscosity, δ_{ij} the Kronecker symbol and $\bar{S}_{ij} = (\partial \bar{u}_i / \partial x_j + \partial \bar{u}_j / \partial x_i) / 2$ the strain-rate tensor. The sgs-viscosity is modeled by the dynamics Smagorinsky-Lilly sgs-model proposed by [Lilly \(1992\)](#). The filtered equation of the conservation of energy is defined as

$$\frac{\partial \bar{\Theta}^L}{\partial t} + \bar{u}_j^L \frac{\partial \bar{\Theta}^L}{\partial x_j} = \alpha \frac{\partial^2 \bar{\Theta}^L}{\partial x_j \partial x_j} - \frac{\partial \bar{u}_i'' \bar{\Theta}''^L}{\partial x_j} \quad (7)$$

where

$$\bar{u}_i'' \bar{\Theta}'' = \bar{u}_i \bar{\Theta} - \bar{u}_i \bar{\Theta} \quad (8)$$

is the sgs-heat flux and α the thermal diffusivity. $\bar{u}_i'' \bar{\Theta}''$ is modeled with the sgs-thermal diffusivity assumption, defined as

$$\bar{u}_i'' \bar{\Theta}'' = \alpha_{sgs} \frac{\partial \bar{\Theta}}{\partial x_i} \quad (9)$$

where $\alpha_{sgs} = \nu_{sgs} / Pr_T$ is the sgs thermal diffusivity and Pr_T the sgs Prandtl number.

In the inner domain, the LES equations for the conservation of momentum and energy are modified to include a implicit blending procedure. They are defined as:

$$\begin{aligned} \frac{\partial \bar{u}_i^S}{\partial t} + \bar{u}_j^S \frac{\partial \bar{u}_i^S}{\partial x_j} &= -\frac{1}{\rho_0} \frac{\partial \bar{p}^S}{\partial x_i} + \nu \frac{\partial^2 \bar{u}_i^S}{\partial x_j \partial x_j} - \frac{\partial \tau_{ij}^S}{\partial x_j} \\ &\quad + (1 - \beta (\bar{\Theta}^S - \bar{\Theta}_0^S)) g_i \\ &\quad + \frac{w}{\tau_R} (\bar{u}_i^L - \bar{u}_i^S) \end{aligned} \quad (10)$$

$$\begin{aligned} \frac{\partial \bar{\Theta}^S}{\partial t} + \bar{u}_j^L \frac{\partial \bar{\Theta}^S}{\partial x_j} = & \alpha \frac{\partial^2 \bar{\Theta}^S}{\partial x_j \partial x_j} - \frac{\partial \bar{u}_j'' \bar{\Theta}''^S}{\partial x_j} \\ & + \frac{w}{\tau_R} \left(\bar{\Theta}^L - \bar{\Theta}^S \right). \end{aligned} \quad (11)$$

The last RHS terms of Equations 10 and 11 are responsible for the implicit blending. The blending is active in the vicinity of the nested boundaries, $60m$ inside the inner domain. In this region, the blending smoothen the transition between the coarse-grained and the fine-grained fields of the L-LES and S-LES respectively. At the nested boundaries $w = 1$ and at the edge of the blending region w is set to 0. The relaxation time τ_R defines the intensity of the blending: the smaller the relaxation time, the stronger the blending. In this case, the relaxation time is set to $\tau_R = 100s$.

The nesting procedure is implemented in a new OpenFOAM solver, available on github¹. The pressure-velocity coupling is handled with the Pressure Implicit with Splitting of Operator (PISO) algorithm, with two pressure correction loops. The conservation of momentum and energy are solved with a preconditioned bi-conjugate gradient (PBiCG) solver and the pressure equation uses a geometric-algebraic multi-grid (GAMG) solver.

The nesting procedure has been validated on simplified geometries by a comparison with reference LES with a fine grid over the whole domain (Vonlanthen et al., 2016) and with wind tunnel measurement performed in the The ETHZ/Empa Atmospheric Boundary Layer Wind Tunnel (Vonlanthen, 2016). The wind tunnel is designed to measure the interaction between the lower part of the ABL and urban configurations (single building or cluster of buildings) or small terrain features. To validate the turbulent ABL, the wind tunnel is equipped with state-of-the-art time-resolved stereoscopic PIV and temperature measurement probe. A complete description of the wind tunnel and the validation experiment is presented in Vonlanthen (2016).

6. Generation of the inflow data for the outer domain

The synthetic turbulent inflow generator proposed by Xie and Castro (2008) is used to generate a time-dependent, fully turbulent velocity field at the south boundary of the outer domain. The generator by Xie and Castro (2008) is similar to the generator proposed by Klein et al. (2003), but with a simplified algorithm, which makes it more efficient in terms of execution time. A detailed comparison of both approach is proposed by Immer (2016). The OpenFOAM implementation of the turbulent inflow generator by Xie and Castro (2008) is proposed by Vonlanthen and Immer (2015).

The profiles for the inflow generator have been extracted from two state-of-the-art LES of a NBL and a CBL. The numerical domain of both simulations covers a flat terrain of $3\text{ km} \times 3\text{ km}$ with a vertical extend of 1.6 km . The grid is composed of three layers. The first layer extends from the ground to 400 m and is made of cubic cells with size of 10 m . The second layer is stacked above the first one, up to 1000 m with cubic cell of 20 m size. The upper most layer fills the domain up to the top boundary with 40 m sized cubic cells.

The ground boundary condition is parametrized with the wall-model proposed by Schumann (1975). The roughness length z_0 is constant over the surface and set to $z_0 = 0.5$. The side boundaries are cyclic and the top boundary is modeled as a free-slip wall. At the startup of both LES, the vertical profile of mean potential temperature $\langle \bar{\Theta} \rangle$ is set to 300 K until 750 m , then followed by an inversion layer of 100 m with a positive temperature gradient of 0.08 K/m . Above the inversion, the temperature increases by 3 K per km . The middle of the inversion is at 800 m and defines the height of the ABL. The ground temperature is set to 300 K for the NBL and 306 K for the CBL. The flow in both simulations is driven by a constant pressure gradient. As it will be shown in the next section, the heat transfer from the ground has an important effect on the velocity, covariance and lengthscale profiles in the unstable case. To have a comparison as fair as possible between the neutral and unstable nested cases, the pressure gradient is set to provide a mean wind speed of 5 m/s at 200 m . Fair in the sense that only a limited amount of parameters should change between the two simulations.

For both simulations, the OpenFOAM ABL-LES solver proposed by Churchfield et al. (2010) is used. It solves the Equations 2, 3 and 7. τ_{ij} is modeled with the dynamic Smagorinsky-Lilly sgs-model (Lilly, 1992) and the sgs-heat fluxes are approximated by Eq.9. The Coriolis term is not included in the momentum equation to match the

¹<https://github.com/ETH-BuildingPhysics/ETH-OFTools-2.3.X>

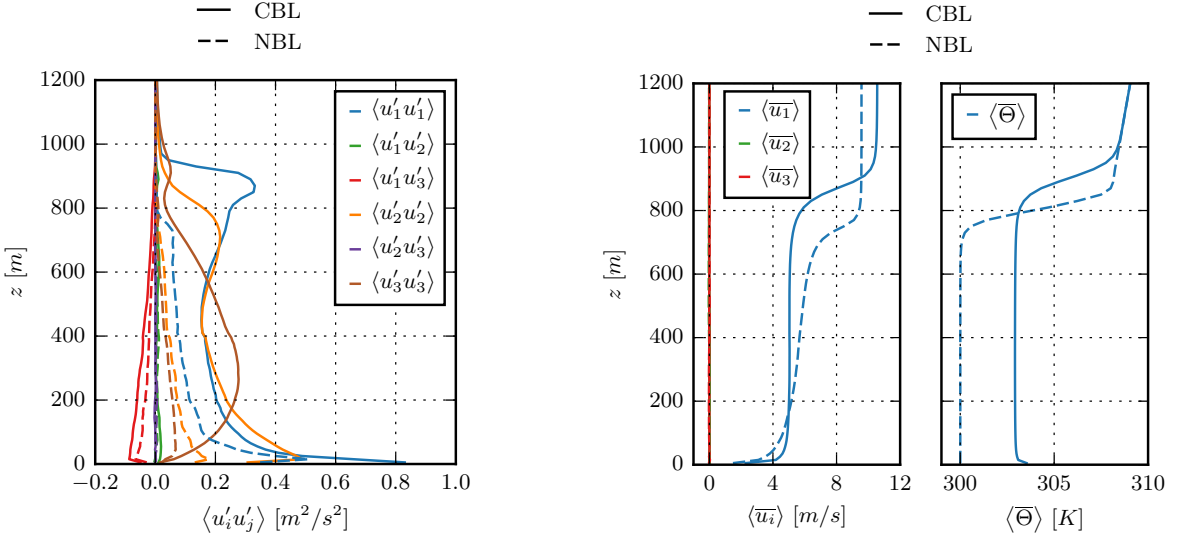


Figure 7: Vertical profile of the Reynolds stress $\langle u'_i u'_j \rangle$. Comparison between the neutral (dashed lines) and the unstable ABL (solid lines).

Figure 8: Vertical mean velocity $\langle \bar{u}_i \rangle$ and temperature profile $\langle \bar{\Theta} \rangle$. Comparison between the NBL (dashed lines) and the CBL (solid lines).

characteristics of the nested simulation defined in Section 5 (cyclic boundary condition non-applicable). Both LES simulate the ABL for 20 hours of physical time. The flow statistics have been computed on a vertical line in the center of the domain using the data of the last 5 hours of physical time. The two-point correlations have been extracted with one point on the central vertical line and the second point moving along the relevant directions.

6.1. Results

The vertical mean velocity $\langle \bar{u}_i \rangle$ and temperature profile $\langle \bar{\Theta} \rangle$ are shown in Figure 8. The CBL is 100 m higher than the NBL. In the LES, nothing stops the CBL from growing, as the turbulence is always feed by the warm ground. In reality, the growth of an CBL would stop in the late afternoon, when the solar forcing reduces. The mixing effect of the CBL is also clearly visible. The streamwise velocity $\langle \bar{u}_1 \rangle$ of the CBL has a very sharp gradient near the ground, and then stays almost constant until the top of the ABL. The same occurs for the temperature: after a strong gradient near the ground, the temperature remains constant up to the ABL top. The velocity profile of the NBL is closer to the well known log-law profile, with a smooth evolution of the speed with respect to the height. As expected, the location of the inversion (80 m) and its strength (0.08 K/m) remain constant in the NBL simulation. The inversion acts as a strong barrier for turbulence between the free atmosphere and the ABL.

The Reynolds stresses are shown in Figure 7. In the CBL, the ABL keeps growing and pushes the inversion higher. Therefore covariances of the CBL from ≈ 750 m to ≈ 1000 m are not valid, as the flow in this layer is statistical non-stationary. The buoyancy mainly influences the three diagonal components of the Reynolds stress tensor. In the CBL, $\langle u'_1 u'_1 \rangle$ is roughly twice bigger than in the NBL. The peak is located at similar height, but with higher intensity. The buoyant effects are even stronger on the component $\langle u'_2 u'_2 \rangle$, which becomes more than four times bigger in the unstable case. The peak value equals $0.45 \text{ m}^2/\text{s}^2$ whereas it is only $0.18 \text{ m}^2/\text{s}^2$ in the neutral case. Higher up, the unstable $\langle u'_2 u'_2 \rangle$ keeps decreasing, but with values much higher than in the neutral case. The most interesting effects of buoyancy are visible on the vertical turbulent flux $\langle u'_3 u'_3 \rangle$. Whereas this Reynolds stress component stays rather small in the neutral case, it becomes one of the most important one in the unstable case. The peak is shifted to 300 m and equals to $0.5 \text{ m}^2/\text{s}^2$. In the neutral case, the peak of $\langle u'_3 u'_3 \rangle$ is reached at 50 m, with a value of $0.08 \text{ m}^2/\text{s}^2$, hence more than six times smaller than in the unstable case.

From each ABL, nine lengthscales $L_{i,j}$ can be extracted. $i \in [1, 2, 3]$ represents the spatial direction and $j \in [1, 2, 3]$ the velocity component. For example, the lengthscales $L_{12,1}$ can be interpreted as the mean size in the spanwise

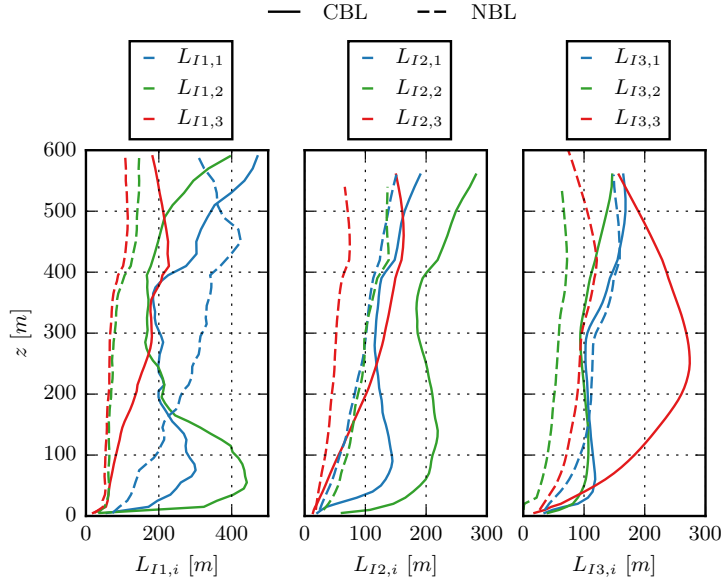


Figure 9: Vertical profile of the lengthscales $L_{Ii,j}$, where i is the spatial direction and j the velocity component. Comparison between the neutral (dashed lines) and the unstable ABL (solid lines).

direction \mathbf{x}_2 of a *cluster* of streamwise velocity \bar{u}_1 . The term *cluster* can somehow be replaced by *eddy*, even though an eddy is generally pictured as a vortex with a rotation motion. The lengthscales of the NBL and the CBL are shown in Figure 9.

In the streamwise direction ($L_{I1,j}$), the lengthscale $L_{I1,1}$ steadily grows with the altitude, whereas $L_{I1,2}$ and $L_{I1,3}$ stay relatively constant. In the CBL, $L_{I1,1}$ and $L_{I1,2}$ are strongly affected in the first 150 m above the ground. Buoyancy has a smaller effect on $L_{I1,3}$, which grows linearly with the elevation, like in the NBL, but with a more important growth rate. In this lower part of the ABL, the structures are bigger in the spanwise direction than in the other directions, whereas the structures are always oriented along the flow in the NBL. Similar trends can be seen for the three lengthscales in spanwise direction ($L_{I2,j}$). In the NBL, they all grow linearly with the altitude. In the CBL, $L_{I2,1}$ and $L_{I2,j}$ reach a first peak value around 100 m and then remain relatively constant up to 400 m. Higher up, $L_{I2,1}$ and $L_{I2,j}$ start to grow again. The effects of buoyancy are quite different in the vertical direction ($L_{I3,j}$). The lengthscales $L_{I3,1}$ and $L_{I3,2}$ are marginally modified by the convection. The shape of their curves is slightly modified, but the mean value remains similar to their counterpart of the neutral case. Major modifications occur on the $L_{I3,3}$. In the CBL, the peak value of $L_{I3,3}$ is reached around 250 m AGL, with a typical size of 280 m.

The statistics presented in Figures 8 and 7, as well as the lengthscales of Figure 9 are used by the turbulent inflow generator used in the nested simulations of the Hönggberg campus. The inversion layer, and its behavior over the hill of Hönggberg is not well known (does it follow the ground or not?) and would depend on large mesoscale features which are not resolved in the outer LES therefore the statistical profiles are simplified and the inversion is removed. They are presented in Figure 10. The lengthscale profiles used in inflow generator are shown in Figure 11. The profiles are simplified by piecewise linear curves to account for the capabilities of the inflow generator. To reproduce the shape transition from the turbulent ABL to the laminar region aloft, the lengthscales set to zero above $z = 770$ m for the NBL and $z = 800$ m for the CBL.

At the time those simulations were performed, the inflow generator was not able to create a turbulent temperature field. Therefore only the mean temperature profile is enforced in the CBL simulation of the Hönggberg campus. Nevertheless, the velocity-temperature covariances stay very small in the ABL, so the lack of temperature fluctuations at the inlet of the nested simulations should not be problematic. Very recently, a new turbulent inflow generator for scalars (e.g. the temperature) has been proposed by Immer (2016). Such generator could be used in future LES of ABL to take into account the temperature fluctuations or any other scalar fluctuations.

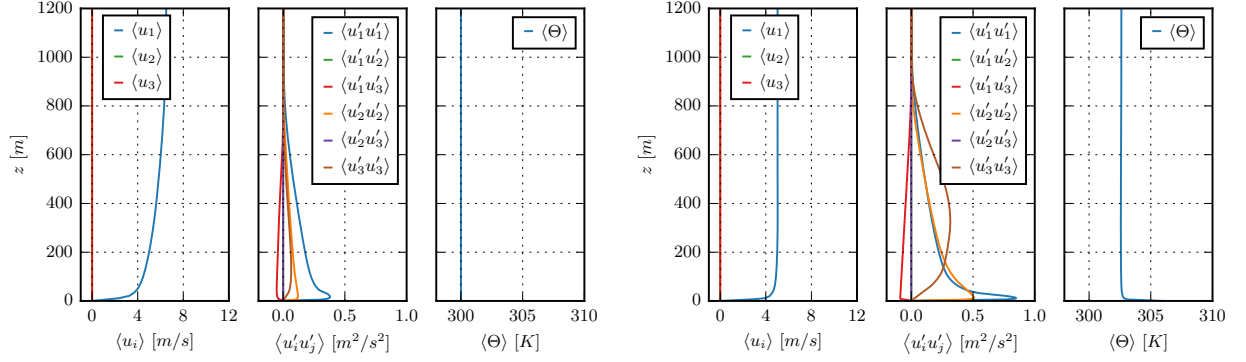


Figure 10: The neutral ABL profiles (a) and The unstable ABL profiles (b) used in the inflow generator of the nested-LES of the Hönggberg campus.

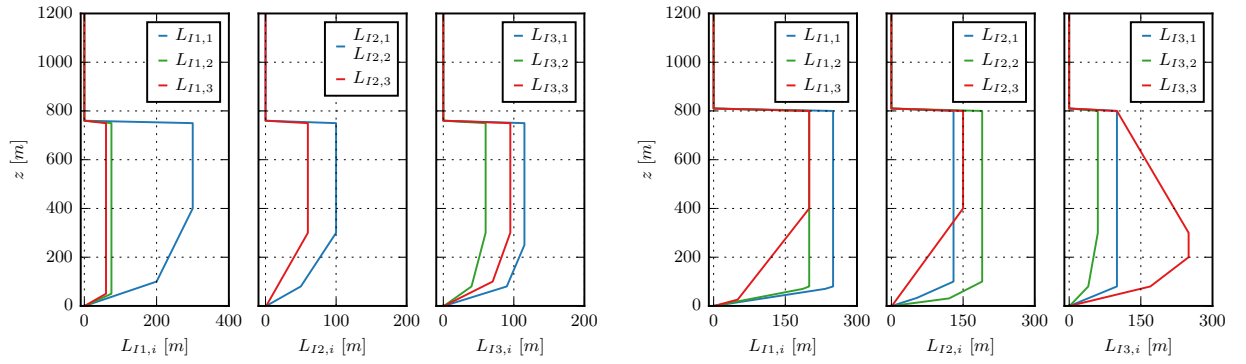


Figure 11: Lengthscale profiles used in the inflow generator for the nested-LES of the Hönggberg campus. NBL lengthscales (a) and CBL lengthscales (b).

7. Results of the nested-LES

In the following sections, the results of the inner and the outer LES of the nested simulations are presented with cut plane images and vertical profiles. All horizontal dimensions are given according the coordinate system [SN,WE] defined in Figure 1. The results extracted from terrain-following cut-planes are oriented like on a map, hence north on the top and west on the left. In those images the flow goes from the bottom to the top (south to north).

In the NBL and the CBL LES, 15 hours of flow are simulated. The first 10 hours are used to spin-up the simulations and the last 5 hours are used to extract the statistics. With this procedure, the flow is fully converged in the both inner and outer domain. The nested-LES needs a shorter spin-up time than the flat terrain LES as the flow entering in the domain is already fully turbulent due to the inflow generator.

7.1. Large scale LES

As seen in the flat terrain simulation used to generate the inflow statistics, buoyancy has a large effect on the shape and the size of the turbulent structures. Figure 12 shows the vertical velocity fluctuations \bar{u}_3' , on a vertical cut-plane aligned with the axis SN and cutting the outer domain of the NBL and CBL in the middle, at $EW = 0\text{ m}$. The blue

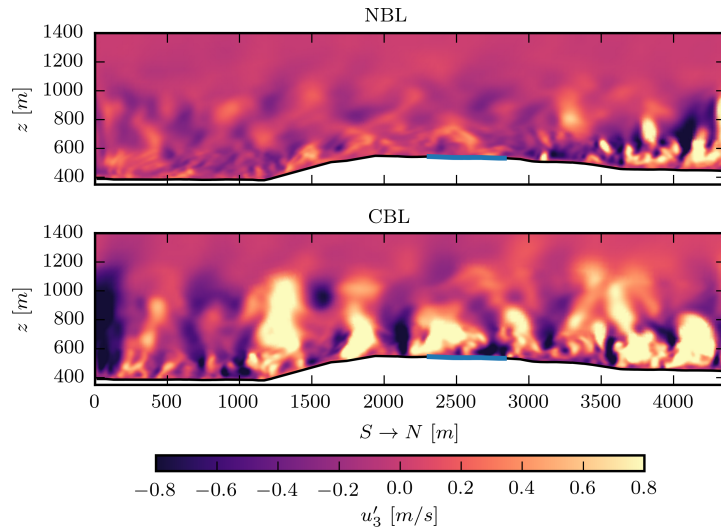


Figure 12: Vertical velocity fluctuations \bar{u}_3' . Streamwise vertical cut-plane at $E \rightarrow W = 0\text{ m}$. The blue part of the ground line indicates the location of the campus.

part of the ground line indicates the location of the campus. From the inlet of the domain to the approximatively $SN = 2800\text{ m}$, the differences between the mechanically driven turbulence (neutral ABL) and the buoyant driven turbulence (unstable ABL) are clearly visible. The CBL is populated with vertically elongated structures with upstream fluctuations. Those structures, generally known as thermics, extend from the ground to the top of the ABL ($\approx 900\text{ m}$ height) and are 100 to 200 m wide in the streamwise direction. The turbulent structures in the NBL grow with the elevation, without showing a real anisotropy in shape. In the neutral case, roughly 500 m after the campus patch, thermics-like structures start to develop. 1000 m after the campus, those new thermics are already 400 m tall, which is roughly the half of the total ABL height. Those structures found their origin in the heating up of the air flowing over the campus area. In the CBL, the added energy from the campus patch does not significantly affect the turbulent structures in the upper part of the ABL.

Figure 13 shows the vertical velocity fluctuations \bar{u}_3' on the terrain-following plane, placed at 100 m AGL. The location of the campus patch is highlighted in gray. In the NBL, the turbulent structures of vertical fluctuations are elongated in the streamwise direction and stay rather thin in the spanwise direction. In the wake of the campus patch, the vertical fluctuations become more intense and the shape of the structure changes. The newly created structures are similar, although smaller, than the buoyant eddies visible in the CBL. Large buoyant structures are visible in the

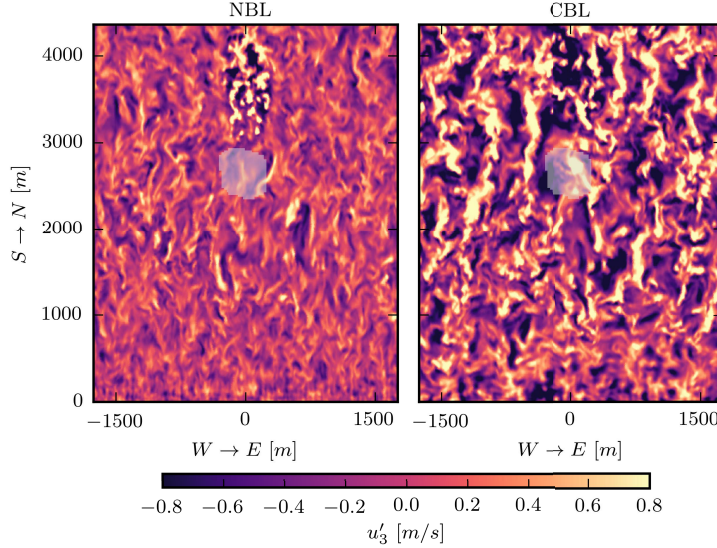


Figure 13: Vertical velocity fluctuations \bar{u}_3' . Terrain-following cut-plane at 100 m AGL. The location of the campus patch is highlighted in grey.

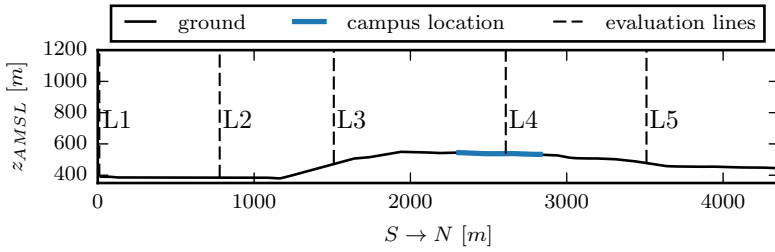


Figure 14: Location of the vertical lines used to extract statistical profiles.

CBL (right plot of Figure 13). They can extend over 1000 m in the streamwise direction and 200 m in the spanwise direction. As already observed in Figure 12 the effect of the thermal plume produced by the campus patch is not clearly visible.

The evolution of the ABL statistics of the vertical profiles through the outer domain is presented in Figures 15 and 16. The data are extracted for five vertical lines L1 to L5, which are located on the vertical streamwise cut-plane $EW = 0$ m (see Figure 14). In the following figures, the profiles are shown with respect to the AGL elevation. The three first lines are located upstream the campus, with the third one on the windward slope of the hill. The fourth line is placed in the middle of the campus patch and the last line is placed in the leeward side of the hill.

The evolution of the NBL and the CBL mean streamwise velocity profiles $\langle \bar{u}_1 \rangle$ along the lines L1 to L5 are given in Figure 15. From the inlet line L1 to line L2, the mean velocity profiles do not evolve a lot, which is expected according to the flat topology and the homogeneous land usage of the alluvial plain. On the windward side of the hill, at the line L3, the flow accelerates, especially in the first 50 m above the ground, where it gains about 1 m/s in both cases. Above the campus patch, at line L4, the profile of the neutral case is similar to the one of the unstable case up to a height of 150 m AGL. This is likely due to the acceleration phase experienced in the windward side of the hill. The Reynolds number can be computed by using the average building height ($h_b \approx 25$ m), viscosity of the air ($\nu = 1.56 \times 10^{-5}$ m²/s) and the mean velocity extracted upstream of the campus patch ($U_r \approx 5$ m/s for both NBL and CBL). This particular location is selected to extract the mean velocity for the Reynolds number because the same location can be used in both domains. This leads to a Reynolds number for the L-LES of $Re^L \approx 8 \times 10^6$ in the outer domain for both NBL and CBL. On the leeside of the hill (line L5), the NBL profile has the typical characteristics of

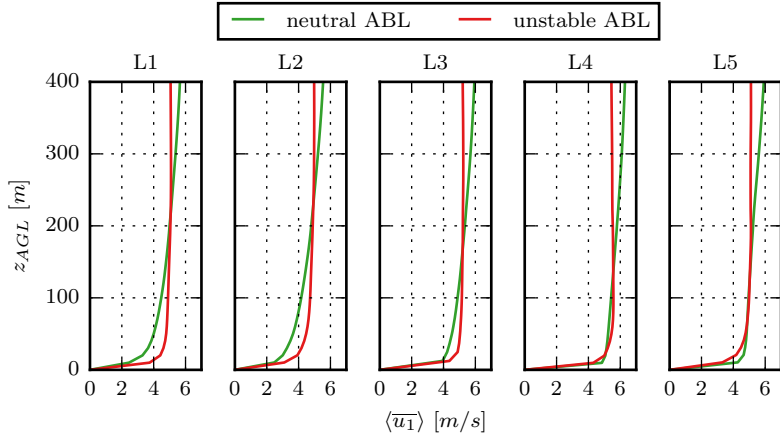


Figure 15: Mean streamwise velocity profiles $\langle u_1 \rangle$ along the lines L1 to L5.

an unstable ABL: a strong velocity gradient at the ground followed by a range of almost constant velocity. Above a height of 200 m AGL, the velocity profile of the neutral case is non perturbed by the convective plume of the campus.

The profiles of the vertical turbulent fluxes are presented in Figure 16. The profile of L1 shows the statistics

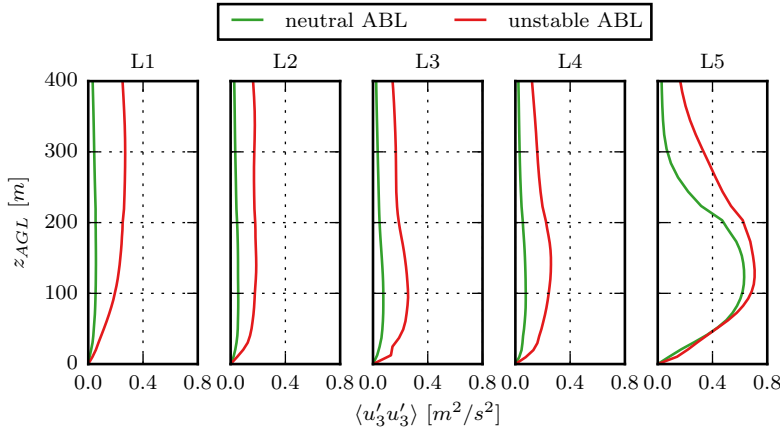


Figure 16: Profiles of the vertical turbulent fluxes $\langle u'_3 u'_3 \rangle$ along the lines L1 to L5.

prescribed by the turbulent inflow generator. Line L2 is located 800 m downstream the first line. The curves at L1 and L2 for the neutral case are similar, whereas the intensity of $\langle u'_3 u'_3 \rangle$ in the unstable case decreases by 1/4 between the first and the second line. Between those two lines, the terrain is flat (alluvial plain) and its land usage is modeled by a constant roughness of $z_0 = 1.5$. The statistics imposed by the inflow generator were generated from the precursor LES presented in Section 6.1, which models the ground with a roughness of $z_0 = 0.5$. It is therefore expected that the bottom part of the profile evolves. In this case, the lower $\langle u'_3 u'_3 \rangle$ above a height of 150 m AGL are due to turbulence reconstruction. Indeed, the turbulence generated at the inflow matches the required statistics, but it is still synthetic turbulence (hence, non physical) and needs a certain distance to develop. According to Immer (2016), two to three ABL heights are needed for a complete reconstruction of turbulence over a flat plat. In this case, the hill shortened this distance, as the topology will trigger new turbulent structures, which enables the possibility to use a shorter inlet fetch. On the windward slope of the hill (line L3), $\langle u'_3 u'_3 \rangle$ increases in the region below a height of 200 m AGL. Whereas the increase due to mechanical turbulence and the slope (neutral case) stays very small, the effect of the buoyancy is much more pronounced (unstable case). Above the campus (line L4), the profiles are relatively similar to the one visible on

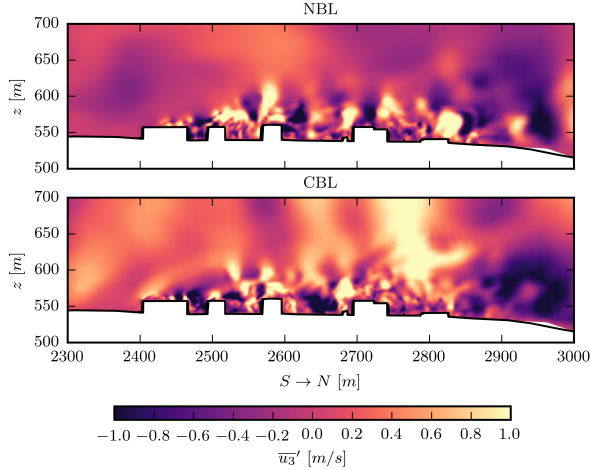


Figure 17: Vertical velocity fluctuations \bar{u}_3' . Streamwise vertical cut-plane at $E \rightarrow W = 0 \text{ m}$.

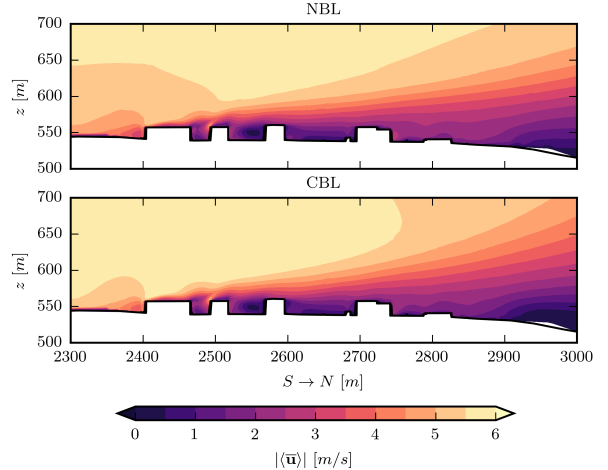


Figure 18: Mean streamwise velocity $|\langle \bar{u} \rangle|$ on the streamwise vertical cut-plane at $E \rightarrow W = 0 \text{ m}$.

the line L3. Downstream the campus patch the effects of the buoyant plume are clearly visible. From 0 m to 100 m , the gradient of $\langle u'_3 u'_3 \rangle$ is similar for NBL and the CBL. Above a height 100 m AGL, the unstable ABL shows higher vertical fluxes than the neutral ABL, and those fluxes remain higher in the rest of the ABL.

The effects of the buoyant plume developing downstream the warm campus patch are important. In the plume, the neutral ABL profile develops the characteristics of a typical unstable ABL: well mixed velocity profiles, large buoyancy-driven turbulent structures and strong vertical turbulence fluxes. 1000 m from the release location, the NBL and CBL are clearly affected by the buoyant plume up to a height of $\approx 400 \text{ m}$ AGL (last plot of Figure 16). The plume is likely to affect the flow several kilometers after its starting point. In a real situation, similar plumes will develop from buildings located upstream the campus and will affect the Honggerberg campus itself. This shows that all the elements surrounding the area of interest may play a significant role and produce buoyant effect, even the ones located several kilometers upstream. For simplicity, the heating up of the area upstream the region of interest is not modeled.

7.2. Small scale LES

The S-LES computes the flow in the inner domain. The grid at the outskirt of the inner domain is similar to the grid of the outer domain (see Figure 6 and 5). Therefore the development of new turbulent structures is not expected in this region. Closer to the buildings, the grid is 8 times finer in every direction than the outer domain grid to be able to capture the small turbulent structures triggered by the buildings. Those new small eddies can easily be identified in Figure 17, which shows the vertical fluctuations on a vertical-cut plane ($EW = 0 \text{ m}$). The new structures have roughly the size of the buildings. They form a *roughness layer*, which extends 2 to 2.5 times the mean building height, $z_b = 20 \text{ m}$ above the ground. The characteristic speed deficit of such layer can be seen in Figure 18. The roughness layer develops from the first buildings and slowly grows until the downstream edge of the campus ($SN = 2820 \text{ m}$), where it reaches a depth of $\approx 3z_b$. After the last building, the growth rate of the roughness sublayer increases due to the downward slope of the hill, which acts as a divergent. Interestingly, both CBL and NBL have a similar roughness layer. Only the wake in the CBL case is slightly thicker. Above the roughness layer, the *outer layer* is visible in Figure 17. This layer is populated by structures of the large scale ABL. In the unstable case, typical elongated clusters of vertical fluctuations start directly above the roughness layer and extends up to the domain top (not visible in the picture).

Inside the roughness layer, the mean velocity magnitude field $|\langle \bar{u} \rangle|$ of the neutral and the unstable case are almost identical, as it can be seen in Figure 19. Inside the campus, the mean velocity magnitude between the buildings is 1 m/s to 2 m/s in average. The recirculation pockets and the areas of higher velocity are very similar for the two cases. The impinging velocity at $SN = 2350 \text{ m}$ (bottom part of the plots in Fig. 19) is equal to 4.5 m/s and is similar in both cases, which explains the similar velocity field in the campus. Looking back at larger scales (Fig. 15), the velocity

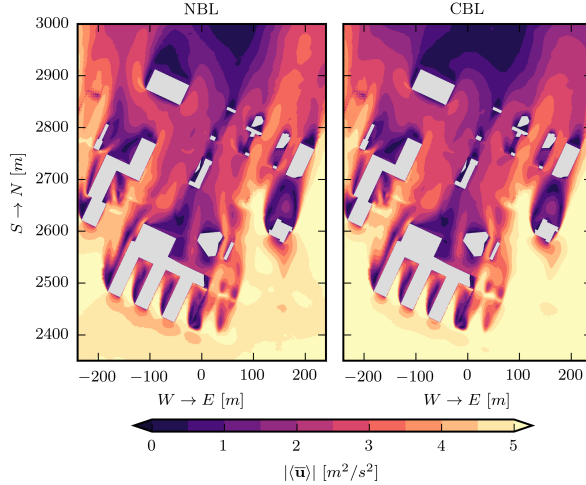


Figure 19: Mean streamwise velocity $|\langle \bar{u} \rangle|$ on the terrain-following cut-plane at 20 m AGL. The campus buildings are displayed in gray.

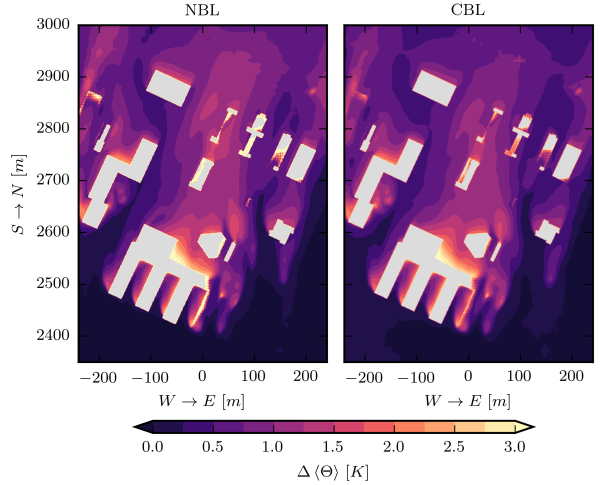


Figure 20: Potential temperature data on a terrain-following cut-plane at 20 m AGL. The mean potential temperature on the line $SN = 2350$ m is used as reference to compute $\Delta(\Theta)$. The campus buildings are displayed in gray.

profile near the ground is almost similar at the evaluation line L4 (located on the campus). Moreover, the grid of the outer domain is made of 10 m tall cells. It means that small variations of velocity in the first 20 m, which would be important at the building level, are simply not captured by the outer domain, and therefore the impinging velocities in the inner domain are identical in both cases. To solve this issue, the upstream part of the inner grid can be refined near the ground, which would help the generation of more realistic wind fluctuations between 0 m to 20 m AGL. The wind velocity in this layer is especially important for wind comfort assessment.

As for the outer L-LES, the Reynolds number of the S-LES is computed with the average building height ($b_r \approx 25$ m), the viscosity of the air ($\nu = 1.56 \times 10^{-5}$ m²/s) and the mean wind velocity extracted upstream of the buildings at 20 m AGL. These numbers give $Re^S \approx 8 \times 10^6$ for both NBL and CBL, which is similar to the L-LES Reynolds number.

Figure 20 shows the potential temperature difference $\Delta\langle\Theta\rangle$ on a terrain-following cut-plane at 20 m AGL. The mean temperature upstream the campus (at $SN = 2350$ m) is used as reference to compute $\Delta\langle\Theta\rangle$. In terms of temperature difference, both cases show similar patterns. In the central part of the campus, the air is 1.25 K to 1.75 K warmer than the air outside the campus. It denotes a small heat island effect as is usually the case un urbanized area.

The stability of the ABL has more consequences on the Reynolds stresses. Figure 21 shows the horizontal turbulent fluxes $\langle u'_1 u'_1 \rangle$. Plumes of high $\langle u'_1 u'_1 \rangle$ are mainly generated at the leading edge of the upstream buildings B1 and B2 in both neutral and unstable case. Inside the campus, the $\langle u'_1 u'_1 \rangle$ turbulent fluxes are higher in the unstable case than in the neutral case. In the wake of the campus, there is an important build up of $\langle u'_1 u'_1 \rangle$. It is likely related to the increasing growth rate of the roughness layer visible in Figure 18.

The vertical turbulent fluxes $\langle u'_3 u'_3 \rangle$ visible in Figure 22 are also mainly generated at the leading edge of the upstream buildings B1 and B2. Those patterns of high $\langle u'_3 u'_3 \rangle$ show larger values in the unstable case. More generally, the intensity of the vertical turbulent fluxes inside the campus are higher in the CBL case than in the NBL.

8. Discussions

As described in Section 5 the S-LES is coupled with the L-LES via the south, east, west and top boundaries, but the north boundary (the outlet) is not coupled. Figure 23 shows the mean velocity magnitude in the neutral case for the S-LES, the L-LES and a third L-LES. The third simulation has the same setup as the L-LES, but with buildings of the campus only crudely resolved. The grid around the building is refined to level L3 (see Tab.4), which means

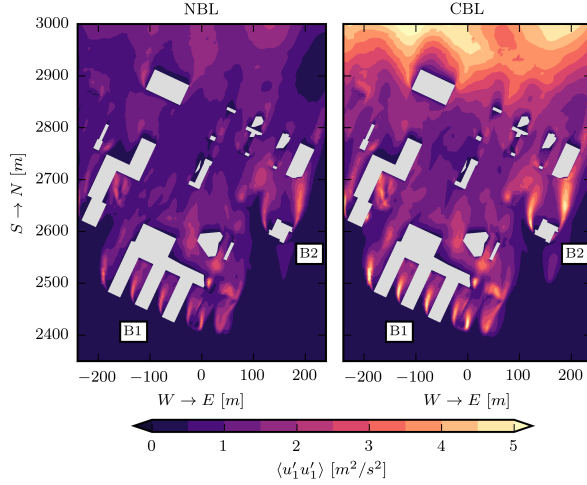


Figure 21: Horizontal turbulent flux $\langle u'_1 u'_1 \rangle$ on the terrain-following cut-plane at 20 m AGL. The campus buildings are displayed in gray.

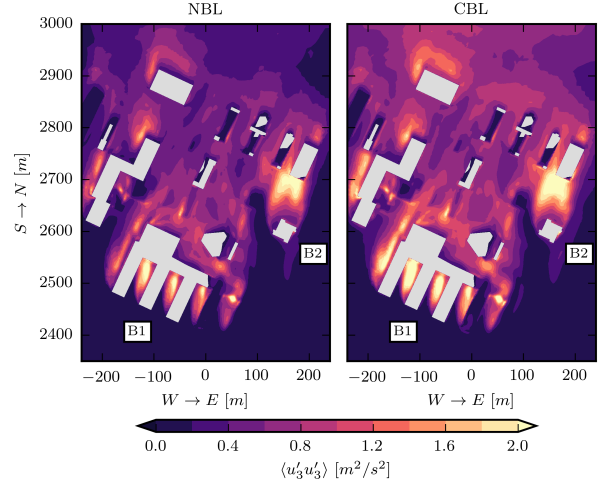


Figure 22: Horizontal turbulent flux $\langle u'_3 u'_3 \rangle$ on the terrain-following cut-plane at 20 m AGL. The campus buildings are displayed in gray.

a cell size of 5 m at the wall. The idea of this simulation is to see which improvement would be achieved when a better *approximation* for the buildings is used. Going back to Figure 23, the roughness layer is clearly missing in the wall-modeled L-LES compared to the S-LES. It is somehow expected, because the wall-models used in ABL-LES are designed to provide the proper surface stresses and fluxes to the outer layer of the ABL, and the flow through the roughness elements is not a concern at such scale. The crudely building-resolved LES shows a better prediction of the roughness layer compared to the wall-modeled L-LES, much closer to the results given by the S-LES. The thickness of the roughness layer is rather well reproduced, but the lack of speed is underestimated in the wake of the campus. From those results, the building-resolved L-LES seems to be a good candidate to serve as the outer domain of the nested simulation. Unfortunately, resolving the buildings, even coarsely, implies a reduction of the timestep by a factor six compared to the wall-modeled L-LES. In other words, a computational time of a nested simulation with the building-resolved L-LES would be much longer compared to the nested setup proposed in this study.

On a larger scale, the effects of the wake downstream the campus buildings can be seen in Figure 24. According to the building-resolved L-LES, the wake affects the flow field up to 1.5 km after the campus location. The wall-modeled L-LES predicts neither the roughness layer, nor the far-field wake. The leading edge of the campus is located only 500 m downstream the last buildings on the SW slope of the Hönggerberg hill (see map on Figure 1). Those buildings upstream are not resolved in the L-LES, but they are likely to generate a roughness layer. This roughness layer may interact with the campus. The wall-model used in the L-LES is not able to reproduce the roughness layer with a reasonable level of accuracy, which can affect the quality of the results in the S-LES, especially in a more integrated situation.

A one-way downscale nested simulation relies heavily on the capabilities of the outer domain to simulate the effect of the parametrized elements (the buildings in this test case) on the flow, which are then resolved in the inner domain. As the area of interest is always located in the first 10 m above the ground, this layer should be reasonably predicted by a computationally efficient wall model. Presently, roughness models for LES cannot reproduce the mean effects of the roughness layer, but better models can be found in operational NWP. However, all those NWP are RANS based solver, therefore their models cannot be directly applied to LES, but can be used as a starting point. For example, Martilli et al. (2002) propose a urban exchange parametrization model for mesoscale NWP, where a urban area is statistically approximated as porous media. Such model could serve as a basis for new LES wall functions, where the roughness layer is correctly reproduced.

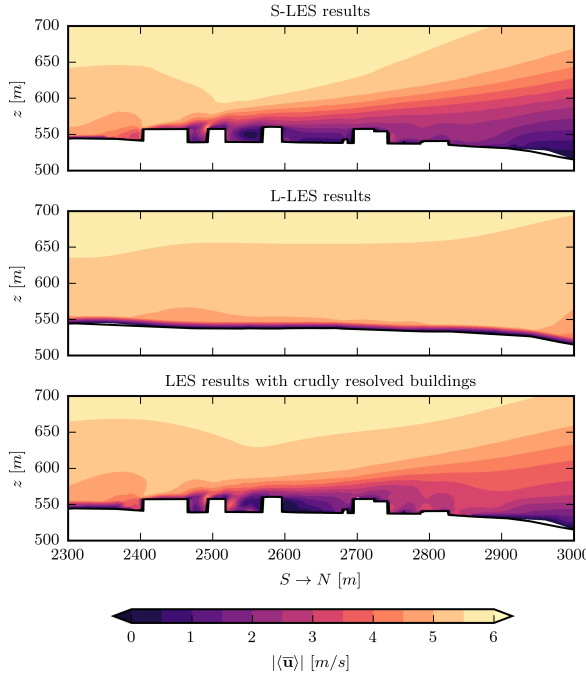


Figure 23: Mean streamwise velocity $|\langle \bar{u} \rangle|$ on the streamwise vertical cut-plane at $E \rightarrow W = 0 \text{ m}$. Comparison of the results between the S-LES, the L-LES and a second L-LES with crudely resolved buildings.

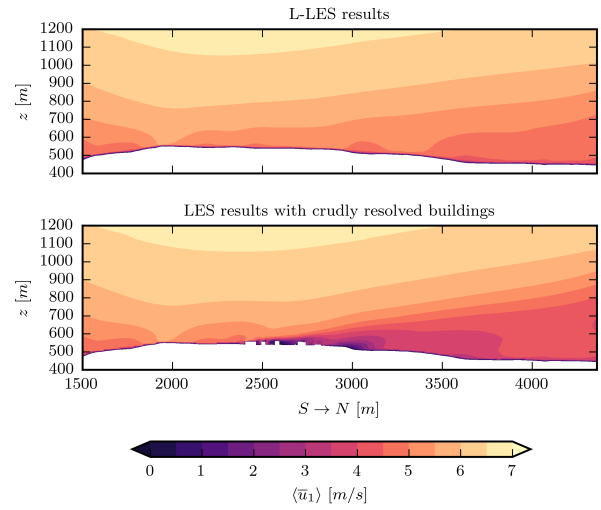


Figure 24: Mean streamwise velocity $|\langle \bar{u} \rangle|$ on the streamwise vertical cut-plane at $E \rightarrow W = 0 \text{ m}$. Comparison of the results between the wall-modeled and the building modeled L-LES.

9. Conclusion

The nesting procedure proposed in Section 5 is successfully applied to a real case scenario. The building of interest and the complex topography around them are included in the nested LES-to-LES simulation presented in this study. The large turbulent scales of the ABL are solved in the outer domain of the nested LES, whereas the small turbulent structures generated by the buildings are solved in the inner domain the nested LES. As the ABL develops over a complex terrain (i.e. not flat and homogeneous), the standard cyclic boundary condition used in standard ABL-LES can not be used. Instead, a synthetic turbulent inflow generator is used to create a time-dependent turbulent flow at the inlet of the outer domain. The statistics of the inflow, used by the turbulence generator, are computed from a standard ABL-LES, over a flat and homogeneous terrain with cyclic boundary conditions.

With this setup, influence of the ABL is clearly visible on the flow through the cluster of buildings. In the CBL case, the intensity of the horizontal turbulent flux $\langle u'_1 u'_1 \rangle$ and the vertical turbulent flux $\langle u'_3 u'_3 \rangle$ increase compared to the NBL case. The difference of potential temperature $\Delta \langle \Theta \rangle$ within the cluster is similar in both NBL and CBL case. Even if the vertical turbulent mixing is higher in the CBL, the heat island effect is equivalent in both cases.

The main issue of such one-way downscale nesting is the capability of the outer domain of the nested-LES to reproduce the effects of the parametrized roughness elements on the flow with a reasonable level of accuracy. Actual LES surface models are only designed to simulate the effects of the ground on the outer layer of the ABL. Therefore, the roughness layer, clearly visible in the inner domain, does not exist in the simulated ABL. New models with a better representation of the roughness layer should be developed for an efficient use of nested-LES and more generally for building resolved LES of urban configurations.

10. Acknowledgment

This study is supported and funded by Swiss Competence Center for Energy and Mobility (CCEM), project no.703: Urban Multiscale Energy Modelling (UMEM).

11. References

- Allegri, J., Dorer, V., Carmeliet, J., 2015. Influence of morphologies on the microclimate in urban neighbourhoods. *Journal of Wind Engineering and Industrial Aerodynamics* 144, 108–117.
URL <http://linkinghub.elsevier.com/retrieve/pii/S0167610515000896>
- Botnick, A. M., Fedorovich, E., 2008. Large Eddy Simulation of Atmospheric Convective Boundary Layer with Realistic Environmental Forcings. *Quality and Reliability of Large-Eddy Simulations* 12, 193–204.
- Churchfield, M. J., Moriarty, P. J., Vijayakumar, G., Brasseur, J. G., 2010. Wind Energy-Related Atmospheric Boundary Layer Large-Eddy Simulation Using OpenFOAM. In: American Meteorological Society. pp. 1–26.
URL <http://ams.confex.com/ams/19Ag19BLT9Urban/techprogram/paper{ }172636.htm>
- Davenport, A. G., 1960. Rationale for determining design wind velocities. *Journal of the Structural Division* 86 (5), 39–68.
- Holtslag, A., Nieuwstadt, F., 1986. Scaling the atmospheric boundary layer. *Boundary-Layer Meteorology* 36 (1-2), 201–209.
- Immer, M., 2016. Time-Resolved Measurement and Simulation of Local Scale Turbulent Urban Flow. Ph.D. thesis, ETH Zurich.
- Kaimal, J. C., 1973. Turbulence spectra, length scales and structure parameters in the stable surface layer. *Boundary-Layer Meteorology* 4 (1-4), 289–309.
- Klein, M., Sadiki, A., Janicka, J., 2003. A digital filter based generation of inflow data for spatially developing direct numerical or large eddy simulations. *Journal of Computational Physics* 186, 652–665.
- Lilly, D. K., 1992. A proposed modification of the Germano subgrid-scale closure method. *Physics of Fluids A: Fluid Dynamics* 4 (3), 633.
URL <http://scitation.aip.org/content/aip/journal/pofa/4/3/10.1063/1.858280>
- Martilli, A., Clappier, A., Rotach, M. W., 2002. An Urban Surface Exchange Parameterisation for Mesoscale Models. *Boundary-Layer Meteorology* 104, 261–304.
- Moeng, C.-H., 1984. A Large-Eddy-Simulation Model for the Study of Planetary Boundary-Layer Turbulence. *Journal of the Atmospheric Sciences* 41 (13), 2052–2062.
- Noh, Y., Cheon, W., Hong, S., Raasch, S., 2003. Improvement of the K-profile model for the planetary boundary layer based on large eddy simulation data. *Boundary-layer meteorology* 107 (2), 401–427.
URL <http://link.springer.com/article/10.1023/A:1022146015946>
- Richards, P. J., Norris, S. E., apr 2011. Appropriate boundary conditions for computational wind engineering models revisited. *Journal of Wind Engineering and Industrial Aerodynamics* 99 (4), 257–266.
URL <http://linkinghub.elsevier.com/retrieve/pii/S0167610510001418>
- Schumann, U., 1975. Subgrid Scale Model for Finite Difference Simulations of Turbulent Flows in Plane Channels and Annuli. *Journal of Computational Physics* 18 (4), 376–404.
- Sullivan, P. P., McWilliams, J. C., Moeng, C.-h., 1994. Subgrid-Scale Model for Large-Eddy Simulation of Planetary Boundary-Layer Flows. *Boundary-Layer Meteorology* 71, 247–276.
- Sullivan, P. P., McWilliams, J. C., Moeng, C.-H., Jul. 1996. A grid nesting method for large-eddy simulation of planetary boundary-layer flows. *Boundary-Layer Meteorology* 80 (1-2), 167–202.
URL <http://link.springer.com/10.1007/BF00119016>
- Vonlanthen, M., 2016. Multiscale and Turbulent Interactions for Urban Microclimate Prediction. Ph.D. thesis, ETH Zurich.
- Vonlanthen, M., Allegri, J., Carmeliet, J., 2016. Assessment of a one-way nesting procedure for obstacle resolved large eddy simulation of the ABL. *Computers & Fluids* 140, 136–147.
- Vonlanthen, M., Immer, M., 2015. Eth-of-tools-2.3.x version 1.0. <https://github.com/ETH-BuildingPhysics/ETH-OFTools-2.3.X>, accessed: 2015-10-1.
- Wieringa, J., 1992. Updating the Davenport roughness classification. *Journal of Wind Engineering and Industrial Aerodynamics* 41 (1-3), 357–368.
- Wyngaard, J., 2010. Turbulence in the Atmosphere. Cambridge University Press.
URL www.cambridge.org/9780511763991
- Xie, Z.-T., Castro, I. P., apr 2008. Efficient Generation of Inflow Conditions for Large Eddy Simulation of Street-Scale Flows. *Flow, Turbulence and Combustion* 81 (3), 449–470.
URL <http://www.springerlink.com/index/10.1007/s10494-008-9151-5>